Bulk and surface electronic properties of SmB_6: A hard x-ray photoelectron spectroscopy study

Y. Utsumi,[1,*] D. Kasinathan,[1] K.-T. Ko,[1] S. Agrestini,[1] M. W. Haverkort,[1,†] S. Wirth,[1] Y-H. Wu,[2] K-D. Tsuei,[2] D-J. Kim,[3] Z. Fisk,[3] A. Tanaka,[4] P. Thalmeier,[1] and L. H. Tjeng[1]

[1]*Max Planck Institute for Chemical Physics of Solids, Nöthnitzer Straße 40, 01187 Dresden, Germany*

[2]*National Synchrotron Radiation Research Center, 101 Hsin-Ann Road, Hsinchu 30077, Taiwan*

[3]*Department of Physics and Astronomy, University of California, Irvine, California 92697, USA*

[4]*Department of Quantum Matter, AdSM, Hiroshima University, Higashi-Hiroshima 739-8530, Japan*

(Received 5 May 2017; revised manuscript received 22 August 2017; published 18 October 2017)

We have carried out bulk-sensitive hard x-ray photoelectron spectroscopy measurements on *in situ* cleaved and *ex situ* polished SmB_6 single crystals. Using the multiplet structure in the Sm $3d$ core level spectra, we determined reliably that the valence of Sm in bulk SmB_6 is close to 2.55 at ~5 K. Temperature dependent measurements revealed that the Sm valence gradually increases to 2.64 at 300 K. From a detailed line shape analysis we can clearly observe that not only the $J = 0$ but also the $J = 1$ state of the Sm $4f^6$ configuration becomes occupied at elevated temperatures. Making use of the polarization dependence, we were able to identify and extract the Sm $4f$ spectral weight of the bulk material. Finally, we revealed that the oxidized or chemically damaged surface region of the *ex situ* polished SmB_6 single crystal is surprisingly thin, about 1 nm only.

DOI: 10.1103/PhysRevB.96.155130

I. INTRODUCTION

The interplay of strong spin-orbit coupling and electron-electron correlations in rare earth compounds has recently been shown theoretically to allow for the emergence of topologically nontrivial surface bands, thereby merging the fields of strongly correlated systems and Kondo physics with topology. A minimum model consisting of localized f electrons and dispersive conduction electrons with opposite parity provides us a f-electron system that hosts topologically protected metallic surface states within a hybridization gap of a Kondo insulator [1].

In this context, it was proposed [1–6] that the Kondo insulator, or intermediate valent system, SmB_6 is a good candidate material to qualify as the first strongly correlated topological insulator. Indeed, the robust metallicity which is attributed to a protected surface state could be a promising explanation for the long-standing mysterious low-temperature residual conductivity of SmB_6 [7–9]. SmB_6 has therefore triggered a tremendous renaissance in recent years, and many research efforts have been made to establish the topological nature of the material using a wide range of experimental methods, e.g., angle-resolved photoelectron spectroscopy (ARPES) [10–15], scanning tunneling spectroscopy [16–20], resistivity and surface conductance measurements [21–28], and high pressure experiments [29–31]. A recent special issue with foreword provides an excellent overview of the field [32].

SmB_6 is an intermediate valent compound where the valence number (v) of Sm ion varies between 2+ and 3+ as first observed by x-ray absorption experiments [33]. An early magnetic susceptibility study [34] hinted at a valence of $v \sim 2.6$ while a subsequent x-ray photoelectron spectroscopy (XPS) experiment [35] extracted $v \sim 2.7$ at room temperature. Using Sm L_3 x-ray absorption spectroscopy, the valence numbers $v = 2.6$–2.65 [33], 2.53 at $T = 4.2$ K [36], and 2.52 at $T = 2$ K [37] were determined. A Sm $L_{\gamma 4}$ emission spectroscopy study found $v = 2.65$ at room temperature [38], and a very recent take-off angle photoemission study yielded $v = 2.48$ at 150 K for the bulk [39]. The Sm valence is an important issue for the theory of the proposed topological character of SmB_6. While an *ab initio* based study including the full $4f$-orbital basis predicts the topological insulator phase with $v \approx 2.5$ [4], model calculations for materials with cubic symmetry including only the Γ_8 quartet states proposed a phase diagram in which SmB_6 is expected [5,6] to be a band insulator for $v < 2.56$, and a topological Kondo insulator when $2.56 < v < 3$.

As mentioned above, several experiments have been performed on SmB_6 to estimate the Sm valence. However, the obtained value varies depending on the experimental methods. Here, we performed bulk sensitive hard x-ray photoelectron spectroscopy (HAXPES) to collect the Sm $3d$ core level spectra from which the Sm valence can be determined [39–41]. We utilized the intensities of the multiplet structure of the Sm^{2+} and Sm^{3+} features, and, by doing so, we did not need to model the background and were therefore able to extract more reliably the ratio between the Sm^{2+} and Sm^{3+} signals. Since many of the reported resistivity and surface conductance experiments on SmB_6 [21–28,31] have been carried out at ambient conditions or on samples which were prepared at such conditions, there is also a need to evaluate the effect of ambient conditions on the SmB_6 surface. We therefore performed HAXPES on *in situ* cleaved SmB_6 and *ex situ* polished SmB_6 and compared the results.

II. EXPERIMENT

The experiments have been carried out at the Max-Planck-NSRRC HAXPES station at the Taiwan undulator beamline BL12XU at SPring-8, Japan. The photon beam with $h\nu \sim 6.5$ keV is linearly polarized with the electrical field vector in the plane of the storage ring (i.e., horizontal). Two MB Scientific A-1 HE hemispherical analyzers have been used

*yuki.utsumi@synchrotron-soleil.fr

†Present address: Institute for Theoretical Physics, Heidelberg University, 69120 Heidelberg, Germany.

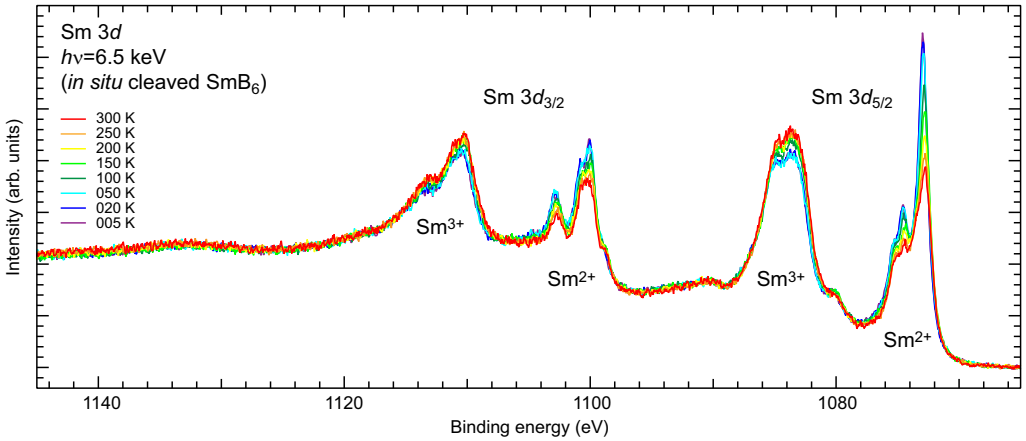

FIG. 1. Temperature dependence of the Sm 3*d* spectra of an *in situ* cleaved SmB_6 single crystal. With increasing temperature, the intensity of the Sm^{2+} (Sm^{3+}) component decreases (increases).

in two different geometries. The first analyzer was mounted horizontally and parallel to the electrical field vector of the photon beam. The second analyzer was in the vertical geometry, perpendicular to the electrical field vector and the Poynting vector of the beam. A detailed description of the experimental setup can be found in Ref. [42]. The overall energy resolution was set to ~170 meV and the zero of the binding energy of the photoelectrons was determined using the Fermi edge of a gold film. The SmB_6 single crystals used in our study were grown by the aluminium flux method [25]. One single crystal was cleaved *in situ* under ultrahigh vacuum conditions (better than 3×10^{-10} mbar). A second single crystal was mirror polished with an Al_2O_3 polishing pad, cleaned using diluted HCl for 2 min, rinsed with isopropanol, and subsequently transferred into the ultrahigh vacuum system. A detailed description of the polishing procedure can be found in Ref. [25].

III. RESULTS AND DISCUSSIONS

A. Sm valence

Figure 1 shows the Sm 3*d* core level spectra of *in situ* cleaved SmB_6 for temperatures ranging from 5 K to 300 K. The Sm 3*d* spectra are split into a $3d_{5/2}$ and a $3d_{3/2}$ branch due to the spin-orbit interaction. Each of these branches is further split into the so-called Sm^{2+} ($4f^6$) and Sm^{3+} ($4f^5$) components which represent the Sm $4f^6 \rightarrow \underline{c}4f^6 + e$ and the Sm $4f^5 \rightarrow \underline{c}4f^5 + e$ transitions, respectively, where $\underline{c}$ denotes a 3*d* core hole and e the outgoing photoelectron. With increasing temperature, the intensity of the Sm^{2+} (Sm^{3+}) component gradually decreases (increases) and, consequently, the mean-valence v of Sm moves towards becoming more trivalent. We would like to note that there were no detectable degradation effects of the sample surface after the temperature cycle; see Appendix A.

In order to obtain v quantitatively, a simulation analysis was performed on the spectra by carrying out atomic full-multiplet calculations to account for the line shape of the Sm 3*d* core level spectra [43,44]. Crystal field effects are not taken into account since the corresponding energy splittings are minute compared to the lifetime broadening of the core-hole final states. The hybridization between the Sm^{2+} and Sm^{3+} core hole final states is neglected in view of the fact that their energy separation is much larger than the hopping integral between the $4f^6$ $J = 0$ and $4f^5$ $J = 5/2$ configurations which is very small due to both the contracted radial wave functions of the Sm $4f$ and fractional-parentage matrix element effects [45]. The calculated spectra are convoluted with a Lorentzian function for lifetime broadening and a Gaussian to account for the instrumental resolution. The experimental spectra at a given temperature are then fitted by adjusting the weights of the calculated Sm^{2+} and Sm^{3+} components such that in the difference spectrum between the experimental and calculated spectra the fingerprints of the Sm^{2+} and Sm^{3+} multiplet structures are minimized. The broadening parameters as well as the values used for the Coulomb and exchange multiplet interactions are listed in Ref. [46].

The results for $T = 5$ K are shown in Fig. 2(a). The experimental spectrum taken at ~5 K (purple line) subtracted by the best fit for the Sm^{2+} (green line) and Sm^{3+} components (brown line) produces a difference spectrum (black line) which shows a gently sloping background plus some residual wiggling features which originate mostly from tiny deviations in the peak positions and peak widths of the multiplet structures. A Sm mean valence of $v = 2.55$ is extracted from this spectrum by using formula $v = 2 + I_{3+}/(I_{2+} + I_{3+})$. Here, I_{2+} and I_{3+} denote the integrated spectral intensities of the Sm^{2+} and Sm^{3+} simulated spectra, respectively, optimized to fit the experimental spectrum.

In the simulations for the higher temperature spectra, we allow for the Boltzmann occupation of the excited states of the Sm. Figure 2(b) displays the results for the $T = 300$ K spectrum. Here we can notice that not only the $J = 0$ (dark green line) but also the $J = 1$ (orange line) state of the Sm^{2+} ($4f^6$) configuration contributes to the spectrum. The energy splitting between the $J = 0$ and $J = 1$ states was set to 35 meV by fine-tuning the $4f$ spin-orbit and multiplet interactions [46] as to match the energy splitting found from inelastic neutron scattering experiments [47,48] resulting in about 57% occupation for the $J = 0$ and 43% for the $J = 1$ states at room temperature. The difference between the experimental spectrum and the multiplet calculation is a gently sloping background curve, similarly smooth like in the 5 K case, demonstrating the validity of the analysis procedure. We stress

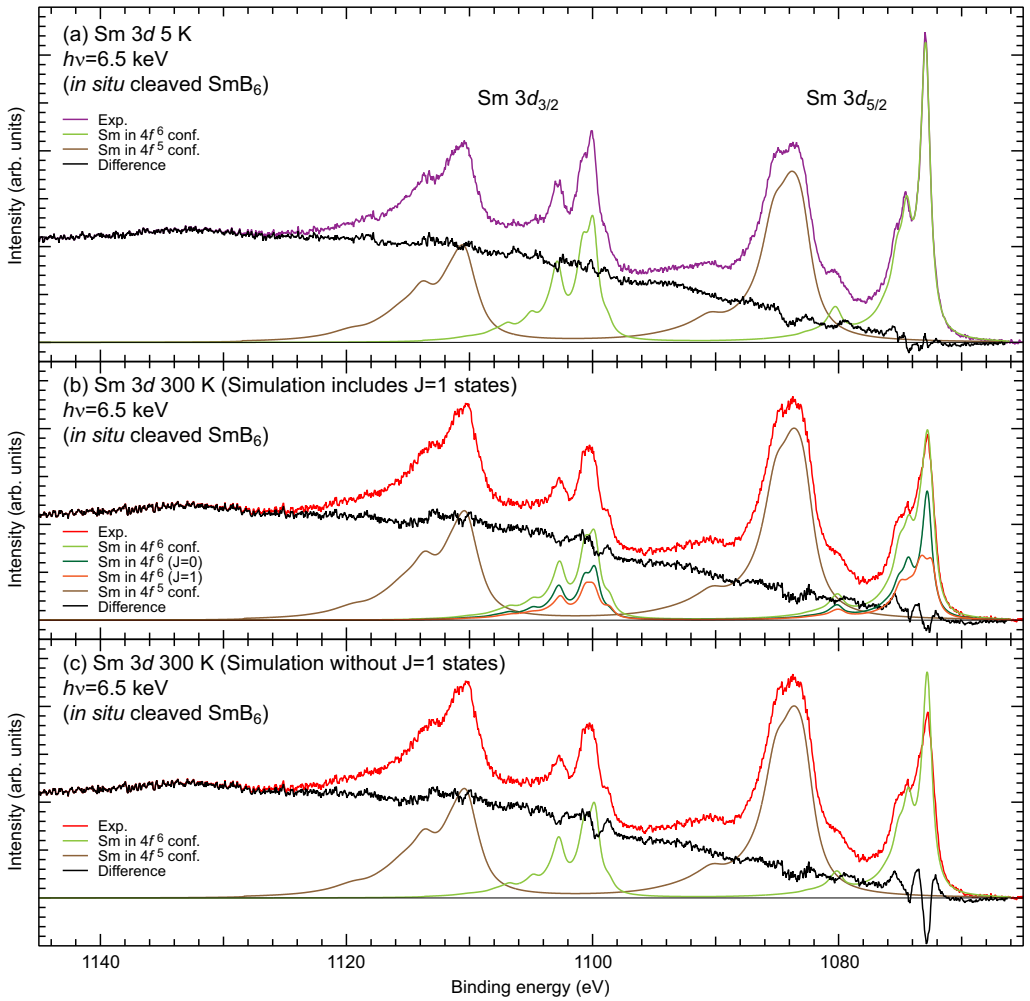

FIG. 2. Multiplet analysis of the Sm 3*d* spectra of the *in situ* cleaved SmB_6 sample. (a) $T = 5$ K, (b) $T = 300$ K including the Boltzmann occupation of the $J = 1$ states of the Sm $^{2+}$ ($4f^6$) configuration in the simulation, and (c) $T = 300$ K without the $J = 1$ states of the Sm $4f^6$. The experimental spectra at 5 K and at 300 K are presented by the purple and red lines, respectively. The simulations for the Sm^{2+} and Sm^{3+} components are displayed by the green and brown lines, and a breakdown of the $J = 0$ and $J = 1$ components of the Sm $^{2+}$ ($4f^6$) configuration by the dark green and orange lines, respectively. Black lines represent the inelastic background signal and were obtained by subtracting the simulated multiplet structure from the experimental spectra.

that in the simulation we cannot omit the $J = 1$ Boltzmann occupation. This is clearly revealed by Fig. 2(c), which shows the poor match between the $J = 0$ only simulation and the experimental spectrum for the Sm^{2+} $3d_{5/2}$. The deviations can also be observed as strong wiggles in the difference spectrum between the experimental and the multiplet calculation.

We would like to remark that for the Sm^{3+} part of the spectrum, the simulations yield a temperature independent line shape for the temperatures considered here. The energy splitting between $J = 5/2$ and $J = 7/2$ multiplets is too large to cause an appreciable Boltzmann occupation of the higher lying $J = 7/2$, so that the spectrum is given primarily by the lower lying $J = 5/2$. Inclusion of a cubic crystal field will also not produce a temperature effect, due to the fact that the Γ_8 and Γ_7 crystal field states originate from the same J quantum number, while at the same time the crystal field energy scale is about two orders of magnitude smaller than that of the inverse lifetime of the 3*d* core hole, i.e., any tiny spectral changes due to the crystal field are washed out by the core-hole lifetime broadening; see Appendix B.

Applying this procedure to spectra taken at other temperatures allowed for a determination of the Sm mean valence as a function of temperature. The results are plotted in the main panel of Fig. 3, revealing a gradual increase of the Sm valence to a value of $v = 2.64$ at 300 K. In general, our findings for the Sm valence and its temperature dependence are consistent with the results reported in earlier Sm-$L_{2,3}$ x-ray absorption spectroscopy (XAS) and Sm $L_{\gamma 4}$ emission spectroscopy studies [36–38]. However, our experimental method and analysis are different with implications for the reliability of the extracted values of the valence. The Sm^{2+} and Sm^{3+} components in our photoemission core level spectra are well separated, more so than in the Sm-$L_{2,3}$ and $L_{\gamma 4}$ spectra. In addition, the presence of sharp multiplet structures in the Sm 3*d* spectra allows us to unambiguously assign the Sm^{2+} and Sm^{3+} components, such that their integrated intensities can be determined without having to model the background.

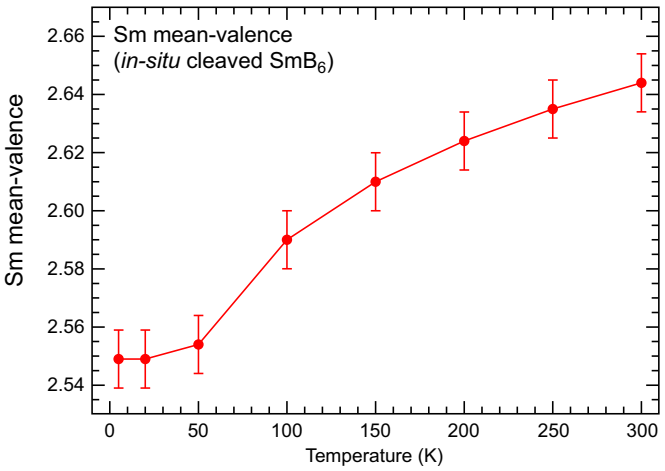

FIG. 3. Temperature dependence of the Sm mean valence of the *in situ* cleaved SmB_6 sample.

TABLE I. Subshell photoionization cross section (σ) at 6.5 keV extrapolated from Refs. [52–54]. σ is divided by the number of electrons in the subshell. β denotes the dipole parameter of the angular distribution. The cross sections for horizontal and vertical geometries are obtained by $\sigma[1+\beta\{1/4+3/4\cos(2\theta)\}]$. Here θ is the angle between the photoelectron momentum and the polarization vector E of the light. In the horizontal and vertical geometries, $\theta = 0^\circ$ and 90°, respectively.

Atomic subshell	σ/e^- (kb)	β	Horizontal (kb)	Vertical (kb)
B $2s$	1.462×10^{-3}	1.945	4.304×10^{-3}	4.037×10^{-5}
B $2p_{1/2}$	6.303×10^{-6}	0.015	6.395×10^{-6}	6.258×10^{-6}
Sm $4f_{5/2}$	4.935×10^{-3}	0.547	7.635×10^{-3}	3.586×10^{-3}
Sm $5p_{1/2}$	8.753×10^{-2}	1.540	0.222	2.011×10^{-2}
Sm $5p_{1/3}$	7.365×10^{-2}	1.634	0.194	1.349×10^{-2}
Sm $6s$	9.467×10^{-3}	1.942	2.785×10^{-2}	2.737×10^{-4}
Sm $5d_{3/2}$	0.013	1.043	2.616×10^{-2}	6.127×10^{-3}

In this way, we also ensure that the multiplet structures are fitted without violating the atomic $3d_{5/2}$ and $3d_{3/2}$ branching ratio (see Appendix C). All this adds to the reliability of the valence determination by performing HAXPES on the $3d$ level. In comparing our HAXPES results with a recent HAXPES take-off angle study carried out at 150 K [39], we would like to note that we have found quite a higher value for the valence, namely $v = 2.61$ at 150 K, while the take-off angle HAXPES provided a value of only $v = 2.48$. Perhaps this is related to the fact that the take-off angle HAXPES study has put more weight in getting a good simulation of the surface sensitive part of the data and thus less on the bulk properties.

One of the interesting findings here is that the low temperature valence of $v = 2.55$ is very close to the border between SmB_6 being a band insulator (for $v < 2.56$) or a topological Kondo insulator (for $2.56 < v < 3$) as pointed out in Refs. [5,6]. If we take these numbers seriously, then it is in fact not clear at all that SmB_6 can be expected to be a strongly correlated topological insulator. However, the critical value $v_c = 2.56$ that separates trivial and topological insulator depends on numerous model parameters and therefore may be subject to fine-tuning. Consequently further investigations, both theoretical and experimental, are clearly warranted.

Another important aspect is the increasing valence with temperature. This effect even outweighs thermal expansion, i.e., the increasing presence of Sm^{3+} (being smaller than Sm^{2+}) causes the lattice constant to shrink with temperature (and correspondingly the linear thermal expansion coefficient to have negative values) for temperatures as high as 150 K [36,49]. The valence is related to the number of $4f$ holes (in the degenerate $J = 5/2$ state) by $n_f^h(T) = v(T) - 2$. Without considering hybridization it becomes entropically favorable to occupy the more degenerate $Sm^{3+}(J = 5/2)$ hole states instead of the Sm^{2+} ($J = 0$) singlet state to decrease the free energy. Therefore, $n_f^h(T)$ and hence the valence $v(T)$ increase with temperature. In a more microscopic picture including the hybridization, a part of the hole spectral weight is pushed above the Fermi level, which leads to a decrease in $n_f^h(T)$ when temperature decreases. This is due to the formation of the bound state of $4f$ hole with a conduction electron as in the case [50] of Yb^{3+}.

B. Valence band

The large inelastic mean-free path of electrons with kinetic energies of several keV [51] provides an opportunity to collect photoemission spectra that are representative of the bulk material by carrying out experiments using hard x-ray photons. The spectra from such HAXPES experiments can then be used as a reference in a comparison with spectra taken at lower photon energies in order to identify features that may originate from the surface region of the sample. In particular, the contribution of the surface may become significant if ultraviolet photon energies are used, as in standard angle-resolved photoelectron spectroscopy (ARPES) experiments [10–15].

At the same time, a HAXPES spectrum of SmB_6 cannot be interpreted as representing directly the Sm $4f$ spectral weight since the photoionization cross section of the Sm $4f$ states is not the only one which contributes to the spectrum. Other states, like the B $2s$ or Sm $5d, 6s$ may also have comparable photoionization cross sections when hard x rays are used [52–54]. Table I lists the photoionization cross sections of the B $2s, 2p$ and Sm $4f, 5p, 5d, 6s$ orbitals as extracted or interpolated from the data [52–54] provided by Trzhaskovskaya *et al.*

In order to extract the more relevant Sm $4f$ spectral weight from HAXPES, we can make use of the pronounced dependence of the spectra on the polarization of the light as given by the so-called β-asymmetry parameter of the photoionization cross sections of the various atomic shells involved [52–54]. They are also listed in Table I. In particular, it has been shown experimentally by Weinen *et al.* [42] that the s contribution to the spectra can indeed be substantially reduced (albeit not completely suppressed due to side-scattering effects) if the direction of the collected outgoing photoelectrons is perpendicular to the electric field vector of the light.

To make use of this polarization dependence we measured the valence band spectra of the *in situ* cleaved SmB_6 crystal

TABLE II. Subshell photoionization cross sections relative to that of Sm $4f$. The horizontal and vertical cross sections in Table I are divided by those of Sm $4f$. The difference values are obtained by subtracting the numbers of the vertical from the horizontal.

Atomic subshell	Horizontal	Vertical	Difference
B $2s$	0.564	1.126×10^{-2}	0.552
B $2p$	8.376×10^{-4}	1.745×10^{-3}	-9.077×10^{-4}
Sm $5p$	2.727×10^{1}	4.686	2.258×10^{1}
Sm $6s$	3.648	7.633×10^{-2}	3.571
Sm $5d$	3.426	1.709	1.718

using the two photoelectron energy analyzers, one positioned in the horizontal geometry and the other mounted in the vertical geometry (see Sec. II). The spectra obtained in this manner are displayed in Fig. 4(a) in red and blue, respectively. The spectra are normalized with respect to the peak height of the features positioned at 0.1 and 1.1 eV binding energy. These features are known to originate from the Sm $4f$ states. We can clearly observe that there is a very strong polarization dependence in a very wide energy region of the spectra, i.e., from 3 eV to 12 eV binding energy. The difference between the two spectra is displayed by the green curve in Fig. 4(b) and has maxima at about 5 and 10 eV.

In order to elucidate the origin of this strong polarization dependence, we have listed in Table I the effective photoionization cross sections for the two geometries and performed band structure calculations using the full-potential nonorthogonal local orbital code (FPLO) [55] to extract the B $2s$, $2p$ and Sm $4f$, $5p$, $5d$, $6s$ partial density of states (PDOS). The local density approximation (LDA) including spin-orbit (SO) coupling was chosen. We considered a nonmagnetic calculation with the Sm $4f^6$ configuration [56], and obtained a total DOS which is quite similar to an earlier calculation for the same Sm configuration [57]. The PDOSs are multiplied by the Fermi function and convoluted with a 0.2 eV FWHM Gaussian broadening, and shown in Fig. 4(b). Here we have weighted the relevant PDOSs with the following factors: from Table I we calculate the photoionization cross sections relative to that of the Sm $4f$, and list them in Table II for each geometry; subsequently, we take the difference of the numbers between the two geometries and use them as multiplication factors for the PDOSs.

Figure 4(b) compares the experimental horizontal-vs-vertical difference spectrum (green line) with the weighted PDOSs. The sum of these weighted PDOSs (black dashed line) is in reasonable agreement with the experiment: the two main maxima at 5 and 10 eV energy are reproduced. The fact that the intensity ratio between these two main maxima does not match well can perhaps be explained by the expected differences in the atomic orbitals used in the photoionization cross-section calculations compared to the ones used in the FPLO band structure code. We should note that we have artificially shifted the results of our calculations by 1 eV towards higher binding energies in order to better align the positions of the main features. This shift may be viewed as an *ad hoc* correction to the band structure calculations which did not take into account

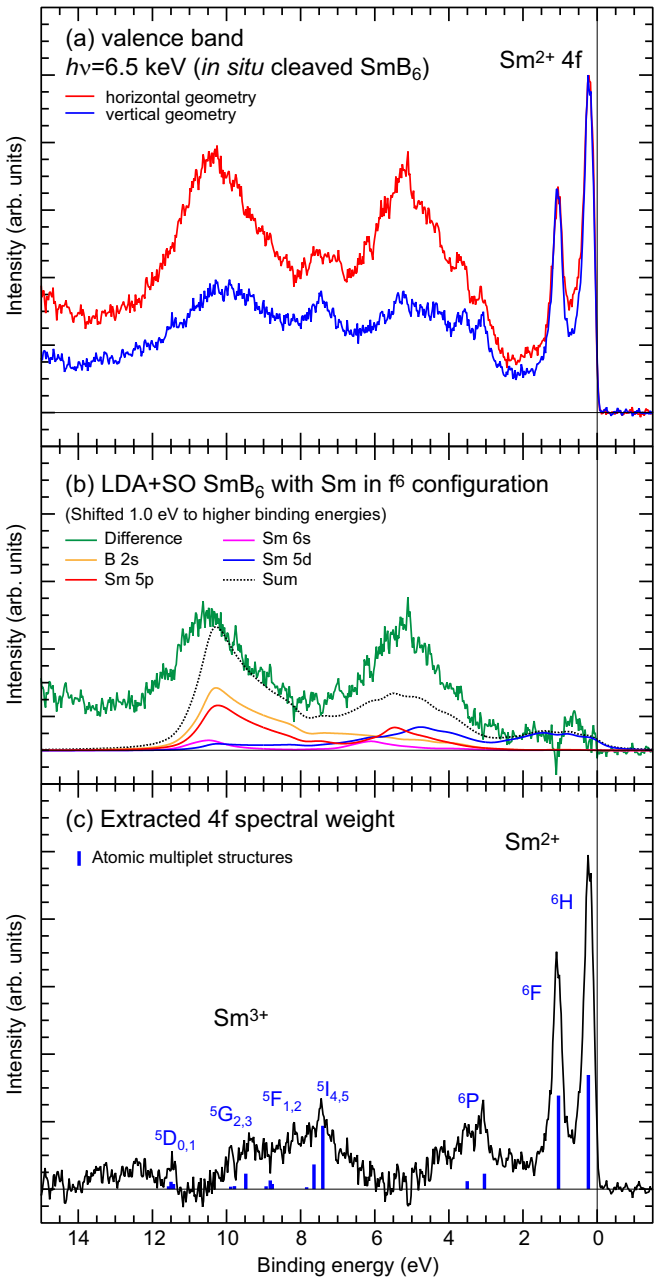

FIG. 4. (a) Experimental valence band spectra of *in situ* cleaved SmB_6 measured in the horizontal (red) and vertical (blue) geometry at $T = 50$ K. The spectra are normalized to the height of the Sm^{2+} $4f$ peaks. (b) Difference between the horizontal and vertical geometry spectra together with the B $2s$ and Sm $5p$, $5d$, $6s$ partial density of states from a nonmagnetic band structure calculation with Sm in the f^6 configuration. The densities of states are displayed with a shift of 1 eV towards higher binding energies and weighted with the photoionization cross-section factors as explained in the text. (c) The experimental valence band spectrum after a weighted (see text) subtraction of the difference spectrum (b) (black line), together with the assignment of the atomic multiplet structures (blue sticks and labels) [14].

the intermediate valent state of Sm. It is also interesting to note that the photoionization cross-section numbers in Tables I and II are extremely large for the Sm $5p$ in comparison to those of the other orbitals. Consequently, the inclusion of the

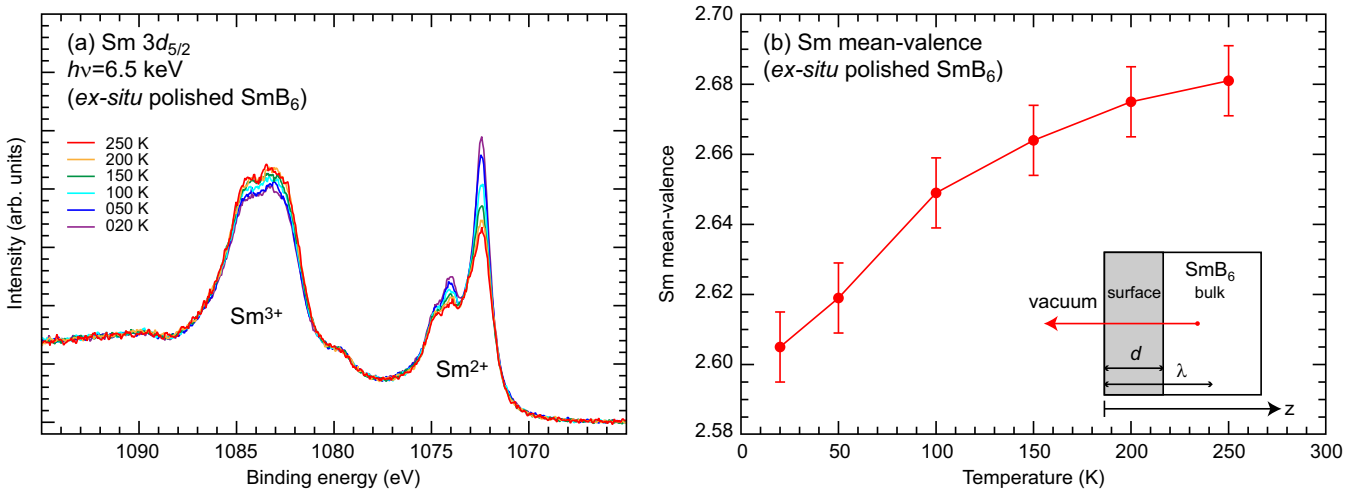

FIG. 5. (a) Temperature dependence of the Sm $3d_{5/2}$ spectra of the *ex situ* polished SmB_6 single crystal. (b) The temperature dependence of the Sm mean valence as extracted from the Sm spectra in (a). The inset shows a schematic model of the bulk and surface regions as used in the fits; see text. Here, d is the thickness of the surface region, λ the inelastic mean-free path of the photoelectrons, and z the distance from the sample surface.

Sm $5p$ becomes important for a quantitative analysis of the valence band HAXPES spectra, although in terms of electronic structure, the contribution of the Sm $5p$ PDOS to the valence band can be safely neglected.

Although the experimental valence band spectrum taken with the vertical geometry as shown in Fig. 4 (blue line) represents already mainly the Sm $4f$ spectral weight (see Tables I and II), we nevertheless can make a further attempt to remove as much as possible the non-$4f$ contribution by carrying out the following exercise: we subtract from the vertical spectrum [I_v, blue line, Fig. 4] the horizontal-vs-vertical difference spectrum [$I_h - I_v$, green line, Fig. 4] multiplied by factor A, and we also subtract from the horizontal spectrum [I_h, red line, Fig. 4(a)] the same horizontal-vs-vertical difference spectrum [$I_h - I_v$, green line, Fig. 4(b)] but now multiplied by factor B, such that the so-obtained spectra are identical: $I_v - A(I_h - I_v) = I_h - B(I_h - I_v)$, i.e., $B - A = 1$. We have found $A = 0.8$ and $B = 1.8$ and we refer to the result as the extracted $4f$ spectral weight represented by the black line in Fig. 4(c). If the orbitals that made up the horizontal-vs-vertical difference spectrum were to have the same β asymmetry parameter, then this procedure will remove the non-$4f$ contributions from the vertical and horizontal spectra. Figure 4(c) displays this extracted $4f$ result (black line), together with the assignments of the atomic multiplet structure (blue sticks and labels) belonging to the photoemission final states which are reached when starting from the Sm^{2+} and Sm^{3+} ground states [14]. We can clearly see that the extracted $4f$ spectral weight spectrum contains most of the sharp multiplet features, not only the high intensity ones at 0.1 and 1.1 eV but also smaller ones in the energy range between 3 and 12 eV. Obviously, there are also some "leftover" intensities that do not match the multiplet structure. As explained above, the subtraction procedure cannot be perfect since the different non-$4f$ orbitals have different β asymmetry parameters (see Table I).

An important result to take from Figs. 4(a) and 4(c) is that there are only two main peaks in the energy range up to 2 eV, namely at 0.1 and 1.1 eV. This is to be contrasted to several photoemission studies using ultraviolet light where the presence of yet another peak at 0.8 eV binding energy has been reported [11,12,14,35]. Based on our HAXPES results, we infer that this 0.8 eV peak very likely originates from the surface region of the SmB_6 material, supporting the assignment made earlier by Allen *et al.* [35]. In fact, the extreme sensitivity of this feature to the experimental conditions [11,14], e.g., the rapid disappearance with time even under ultrahigh vacuum conditions, suggests strongly that the 0.8 eV peak is caused by Sm atoms residing on top of the surface. Given the fact that the (001) surface investigated in the ARPES studies is polar [11], a Sm termination must indeed be accompanied by a substantial electrostatic potential rearrangement for the Sm atoms at the surface. Yet, STM studies also revealed that an unreconstructed Sm-terminated surface is rather rare. Instead, complex ordered and disordered surface structures are more commonly observed [17,19].

C. Surface of *ex situ* polished SmB_6

One can readily expect that the surface of an *ex situ* polished SmB_6 single crystal will be different from the one of an *in situ* cleaved sample. Not only will any Sm present on the surface be oxidized, but also the oxidation process may in principle continue further into the bulk material, thereby creating a thicker surface region in which the Sm may have a valence different from the bulk value. In order to investigate the consequences of an *ex situ* preparation of the samples, we also carried out Sm $3d$ core-level photoemission studies on *ex situ* polished SmB_6 samples.

In Fig. 5(a) the Sm $3d_{5/2}$ spectrum of an *ex situ* polished SmB_6 and its temperature dependence is presented. It exhibits the same Sm^{2+} and Sm^{3+} components with the same temperature tendency as the *in situ* cleaved SmB_6. However, the Sm mean valences are shifted to higher values over the entire temperature range as compared to those of the *in situ* cleaved sample: for the *ex situ* polished SmB_6 we obtained $v = 2.61$

at 20 K and $v = 2.68$ at 250 K; see Fig. 5(b). This is to be compared to 2.55 and 2.64, respectively, for the *in situ* cleaved SmB_6.

Clearly, an analysis of the spectra obtained for the *ex situ* polished SmB_6 sample has now to take into account the possibility of a nonuniform value of v at the surface and in the bulk. To accomplish this, we adopt a minimal model (even simpler than the one used in Ref. [39]) in which we assume that the sample can be divided into two regions, namely the surface region which has the Sm in its fully oxidized 3+ state, $v_{surf} = 3$, and the bulk region which has its pristine intermediate-valence properties v_{bulk}; see the inset of Fig. 5(b). This allows us to set up an equation for the measured average valence v_{av} of the *ex situ* polished SmB_6 taking also into account the probing depth of the photoemission measurement:

$$v_{av}\int_0^\infty e^{-z/\lambda}dz = v_{surf}\int_0^d e^{-z/\lambda}dz + v_{bulk}\int_d^\infty e^{-z/\lambda}dz. \quad (1)$$

Here, λ is the inelastic mean-free path of the photoelectrons, z the distance from the surface, and d the thickness of the surface region. After integration, one can obtain d from

$$\frac{d}{\lambda} = \ln\left[\frac{v_{surf} - v_{bulk}}{v_{surf} - v_{av}}\right]. \quad (2)$$

Using the experimental values of v_{bulk} (Fig. 3) [60] and v_{av} [Fig. 5(b)] [60], as well as an estimated inelastic mean-free path of about ~72 Å for 5.5 keV photoelectrons [51], we arrive at a thickness $d \approx 9.5$ Å using the 20 K data and $d \approx 9.7$ Å at 250 K. Although the employed model is highly schematic and should not be taken literally, it provides the surprising indication that the thickness of the oxidized or chemically damaged surface region of the *ex situ* polished SmB_6 is rather small, about 1 nm. It appears that SmB_6 has a surface which is relatively "leak-tight" against exposure to ambient atmosphere. One then might conjecture that this could explain why many of the conductivity measurements carried out under ambient conditions exhibit a surprisingly high reproducibility [7–9,21–28].

IV. SUMMARY

We have performed bulk sensitive hard x-ray photoelectron spectroscopy measurements on *in situ* cleaved SmB_6 to elucidate the Sm valence and the Sm $4f$ spectral weight of the bulk material. The multiplet structure in the Sm $3d$ core level spectra provides a reliable base for an analysis of the valence. This analysis results in a value of $v = 2.55$ at ~5 K, which is close to the theoretical estimate for the border separating topologically trivial from topologically nontrivial SmB_6. The strong increase of the valence with temperature suggests that this is driven by the entropic gain in free energy due to the higher degeneracy of the magnetic Sm^{3+} $4f^5$ state compared to the nonmagnetic $4f^6$ singlet state of the Sm^{2+}. At elevated temperatures we can clearly observe in our spectra the presence of the Boltzmann occupation of the $J = 1$ state of the Sm $4f^6$ configuration. The strong polarization dependence in the valence band spectra allowed us to extract the Sm $4f$ spectral weight, thereby disentangling surface from bulk contributions to the valence band spectra collected by ARPES. The measurements on *ex situ* polished SmB_6 single crystals revealed an oxidized or chemically damaged surface region which is surprisingly thin, of order 1 nm only.

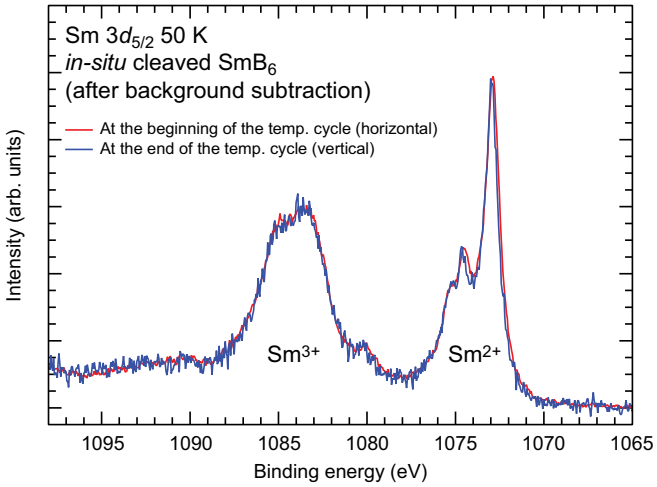

FIG. 6. Sm $3d_{5/2}$ spectra measured at 50 K at the beginning of the experiment (red line) and the end of the temperature cycle (blue line).

ACKNOWLEDGMENTS

We would like to thank T. Mende and C. Becker for their skillful technical assistance and S. Rößler for helpful discussions. D.K. acknowledges funding from the Deutsche Forschungsgemeinschaft (DFG) through SPP 1666. K.-T.K. was supported by Study for Nano Scale Optomaterials and Complex Phase Materials (2016K1A4A4A01922028) through NRF funded by MSIP of Korea.

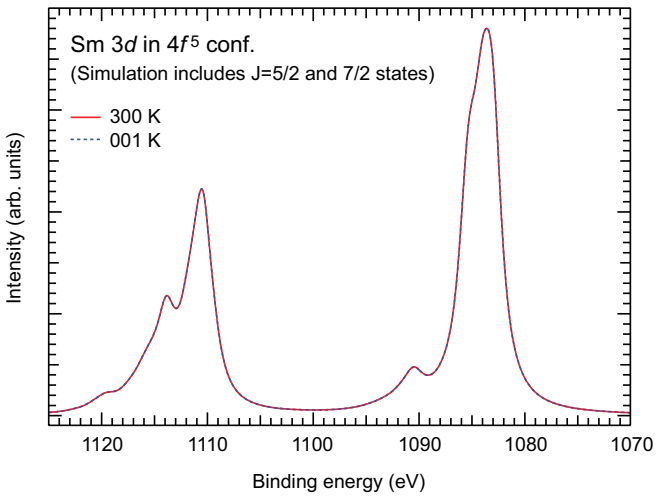

FIG. 7. Calculated Sm $3d$ core-level spectrum for a Sm^{3+} ion at $T = 1$ K (blue dashed line) and $T = 300$ K (red line) with the cubic crystal field for NdB_6 in Ref. [61]. The $J = 5/2$ Γ_8 ground state, the $J = 5/2$ Γ_7 excited state at ~13 meV, and higher lying $J = 7/2$ excited states around 130 meV are included for the initial state (see text). The spectra were convoluted with a Lorentzian function with FWHM = 0.45 eV and a Gaussian function with FWHM = 0.22 eV.

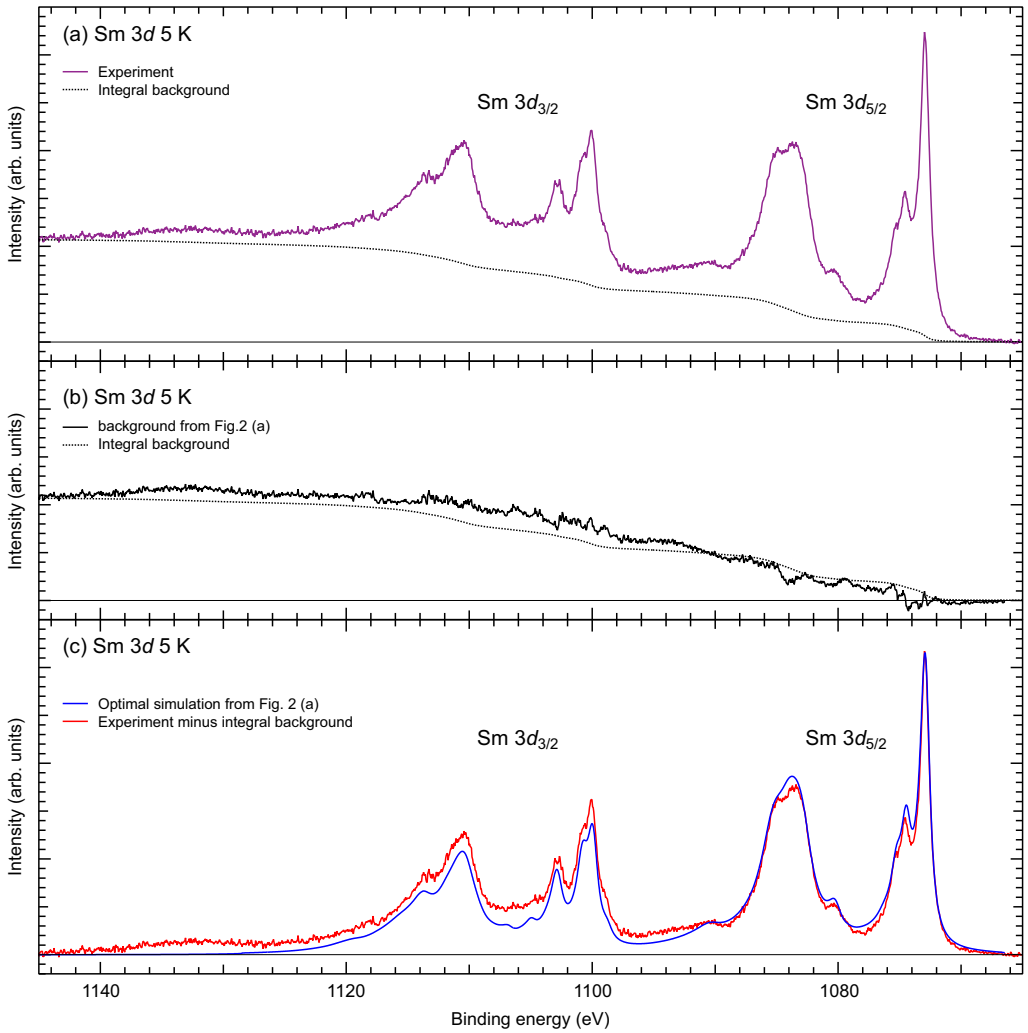

FIG. 8. (a) Experimental spectrum (purple line) of the *in situ* cleaved sample taken at 5 K together with its integral background (black dashed line). (b) Comparison of the integral background (black dashed line) with the background (black line) from Fig. 2. (c) Experimental spectrum corrected for the integral background (red line) and the optimal simulation (blue line) from Fig. 2(a).

APPENDIX A: REPRODUCIBILITY OF THE SM 3*d* SPECTRA

In order to verify the absence of surface degradation effects, we compare in Fig. 6 the Sm $3d_{5/2}$ spectrum measured at 50 K at the beginning of the experiment with the one measured at the very end of the temperature cycle (50 K $\rightarrow$ 20 K $\rightarrow$ 5 K $\rightarrow$ 100 K $\rightarrow$ 200 K $\rightarrow$ 250 K $\rightarrow$ 300 K $\rightarrow$ 50 K). The two spectra reproduce each other, thus demonstrating that surface degradation did not take place and that the observed temperature evolution of Sm 3*d* spectrum is real. The total measurement time for the cycle was 33 h.

APPENDIX B: CRYSTAL ELECTRIC FIELD EFFECT ON THE Sm^{3+} 3*d* SPECTRUM

In the case of Sm f^5 (Sm^{3+}), the lowest $4f$ multiplet states are given by $J = 5/2$ and $J = 7/2$, with the latter about 130 meV higher in energy. A cubic crystal electric field splits $J = 5/2$ further into the quartet Γ_8 and the doublet Γ_7 states. Although the precise value of the crystal field for SmB_6 is still not known, if we adopt the value of the crystal field for NbB_6 determined from inelastic neutron scattering experiments [61], the energy difference between the Γ_8 and Γ_7 states is about 13 meV, which is about one-tenth of that between the $J = 5/2$ and $J = 7/2$ levels.

Assuming the same crystal field, we have calculated the Sm 3*d* core-level spectrum for $T = 1$ K and $T = 300$ K. The results are shown in Fig. 7. In contrast with the Sm^{2+} spectra, where we found the large temperature effects, we here clearly observe that the spectra are practically identical. One reason is that the energy splitting between $J = 5/2$ and $J = 7/2$ is too large to cause an appreciable Boltzmann occupation of $J = 7/2$ for the temperatures considered here, i.e., only $J = 5/2$ contribute to the spectrum. Another reason is that the inclusion of the cubic crystal electric field does not add any noticeable new spectral features due to the fact that the Γ_8 and Γ_7 states originate from the same J quantum number, while at the same time the crystal field energy scale is about two orders of magnitude smaller than that of the inverse lifetime of the 3*d* core hole.

APPENDIX C: BACKGROUND CORRECTION FOR THE Sm 3*d* SPECTRA

The standard procedure in the literature in evaluating the valence of mixed valent strongly correlated systems from core level spectra is to first make a correction for the background signal due to inelastic electron scattering processes, and then to evaluate the intensities of the relevant configurations, in our case, the Sm^{2+} and Sm^{3+}. The problem is that for this procedure to work accurately one needs to know the loss function (in photoemission) in order to know what line shape the background should have. However, the loss function is usually not known and it is a major effort to determine it experimentally. It is obvious that different assumptions for the line shape of the background will lead to different background-corrected spectra and thus likely to different values for the valence. To illustrate the ambiguities that enter when using a background correction procedure, we now apply the generally used integral background correction [62] to our 5 K spectrum; see panel (a) of Fig. 8. It is interesting to note that this integral background shows discrepancies to the background that we have obtained using the multiplet line shape analysis as displayed in Fig. 2; see panel (b) of Fig. 8 and compare the black dashed line with the black line, respectively. Consequently, there are also discrepancies between the integral-background-corrected spectrum and the optimal simulation from Fig. 2; i.e., compare the red line with the blue line, respectively, in panel (c) of Fig. 8. The integral-background-corrected spectrum has in fact intensities over a wide energy range that cannot be accounted for by the multiplet structures. Also the intensity of the $3d_{3/2}$ relative to the $3d_{5/2}$ has increased in the integral-background corrected spectrum in comparison with the multiplet theory, meaning that the integral-background corrected spectrum violates the atomic branching ratio between $3d_{5/2}$ and $3d_{3/2}$ components. This indicates that our multiplet line shape analysis can give a more reliable Sm valence value than the one using integral background.

[1] M. Dzero, K. Sun, V. Galitski, and P. Coleman, Phys. Rev. Lett. **104**, 106408 (2010).
[2] T. Takimoto, J. Phys. Soc. Jpn. **80**, 123710 (2011).
[3] M. Dzero, K. Sun, P. Coleman, and V. Galitski, Phys. Rev. B **85**, 045130 (2012).
[4] F. Lu, J. Z. Zhao, H. Weng, Z. Fang, and X. Dai, Phys. Rev. Lett. **110**, 096401 (2013).
[5] M. Dzero and V. Galitski, J. Exp. Theor. Phys. **117**, 449 (2013).
[6] V. Alexandrov, M. Dzero, and P. Coleman, Phys. Rev. Lett. **111**, 226403 (2013).
[7] J. W. Allen, B. Batlogg, and P. Wachter, Phys. Rev. B **20**, 4807 (1979).
[8] B. Gorshunov, N. Sluchanko, A. Volkov, M. Dressel, G. Knebel, A. Loidl, and S. Kunii, Phys. Rev. B **59**, 1808 (1999).
[9] K. Flachbart, K. Gloos, E. Konovalova, Y. Paderno, M. Reiffers, P. Samuely, and P. Švec, Phys. Rev. B **64**, 085104 (2001).
[10] N. Xu, X. Shi, P. K. Biswas, C. E. Matt, R. S. Dhaka, Y. Huang, N. C. Plumb, M. Radović, J. H. Dil, E. Pomjakushina, K. Conder, A. Amato, Z. Salman, D. McK. Paul, J. Mesot, H. Ding, and M. Shi, Phys. Rev. B **88**, 121102(R) (2013).
[11] Z.-H. Zhu, A. Nicolaou, G. Levy, N. P. Butch, P. Syers, X. F. Wang, J. Paglione, G. A. Sawatzky, I. S. Elfimov, and A. Damascelli, Phys. Rev. Lett. **111**, 216402 (2013).
[12] M. Neupane, N. Alidoust, S.-Y. Xu, T. Kondo, Y. Ishida, D.-J. Kim, C. Liu, I. Belopolski, Y. J. Jo, T.-R. Chang, H.-T. Jeng, T. Durakiewicz, L. Balicas, H. Lin, A. Bansil, S. Shin, Z. Fisk, and M. Z. Hasan, Nat. Commun. **4**, 2991 (2013).
[13] J. Jiang, S. Li, T. Zhang, Z. Sun, F. Chen, Z. R. Ye, M. Xu, Q. Q. Ge, S. Y. Tan, X. H. Niu, M. Xia, B. P. Xie, Y. F. Li, X. H. Chen, H. H. Wen, and D. L. Feng, Nat. Commun. **4**, 3010 (2013).
[14] J. D. Denlinger, J. W. Allen, J.-S. Kang, K. Sun, B.-I. Min, D.-J. Kim, and Z. Fisk, JPS Conf. Proc. **3**, 017038 (2014).
[15] N. Xu, C. E. Matt, E. Pomjakushina, X. Shi, R. S. Dhaka, N. C. Plumb, M. Radović, P. K. Biswas, D. Evtushinsky, V. Zabolotnyy, J. H. Dil, K. Conder, J. Mesot, H. Ding, and M. Shi, Phys. Rev. B **90**, 085148 (2014).
[16] M. M. Yee, Y. He, A. Soumyanarayanan, D.-J. Kim, Z. Fisk, and J. E. Hoffman, arXiv:1308.1085.
[17] S. Rößler, T.-H. Jang, D.-J. Kim, L. H. Tjeng, Z. Fisk, F. Steglich, and S. Wirth, Proc. Natl. Acad. Sci. USA **111**, 4798 (2014).
[18] W. Ruan, C. Ye, M. Guo, F. Chen, X. Chen, G. M. Zhang, and Y. Wang, Phys. Rev. Lett. **112**, 136401 (2014).
[19] S. Rößler, L. Jiao, D.-J. Kim, S. Seiro, K. Rasim, F. Steglich, L. H. Tjeng, Z. Fisk, and S. Wirth, Philos. Mag. **96**, 3262 (2016).
[20] L. Jiao, S. Rößler, D.-J. Kim, L. H. Tjeng, Z. Fisk, F. Steglich, and S. Wirth, Nat. Commun. **7**, 13762 (2016).
[21] M. C. Hatnean, M. R. Lees, D. McK. Paul, and G. Balakrishnan, Sci. Rep. **3**, 3403 (2013).
[22] X. Zhang, N. P. Butch, P. Syers, S. Ziemak, R. L. Greene, and J. Paglione, Phys. Rev. X **3**, 011011 (2013).
[23] D.-J. Kim, S. Thomas, T. Grant, J. Botimer, Z. Fisk, and J. Xia, Sci. Rep. **3**, 3150 (2013).
[24] S. Wolgast, C. Kurdak, K. Sun, J. W. Allen, D.-J. Kim, and Z. Fisk, Phys. Rev. B **88**, 180405 (2013).
[25] D.-J. Kim, J. Xia, and Z. Fisk, Nat. Mater. **13**, 466 (2014).
[26] S. Wolgast, Y. S. Eo, T. Öztürk, G. Li, Z. Xiang, C. Tinsman, T. Asaba, B. Lawson, F. Yu, J. W. Allen, K. Sun, L. Li, Ç. Kurdak, D.-J. Kim, and Z. Fisk, Phys. Rev. B **92**, 115110 (2015).
[27] S. Thomas, D.-J. Kim, S. B. Chung, T. Grant, Z. Fisk, and J. Xia, Phys. Rev. B **94**, 205114 (2016).
[28] Y. Nakajima, P. Syers, X. Wang, R. Wang, and J. Paglione, Nat. Phys. **12**, 213 (2016).
[29] N. P. Butch, J. Paglione, P. Chow, Y. Xiao, C. A. Marianetti, C. H. Booth, and J. R. Jeffries, Phys. Rev. Lett. **116**, 156401 (2016).
[30] L. Sun and Q. Wu, Rep. Prog. Phys. **79**, 084503 (2016).
[31] Y. Zhou, Q. Wu, P. F. S. Rosa, R. Yu, J. Guo, W. Yi, S. Zhang, Z. Wang, H. Wang, S. Cai, K. Yang, A. Li, Z. Jiang, S. Zhang, X. Wei, Y. Huang, Y. F. Yang, Z. Fisk, Q. Si, L. Sun, and Z. Zhao, arXiv:1603.05607.
[32] J. W. Allen, Philos. Mag. **96**, 3227 (2016).
[33] E. E. Vainshtein, S. M. Blokhin, and Y. B. Paderno, Sov. Phys. Solid State **6**, 2318 (1965).

[34] R. L. Cohen, M. Eibshütz, and K. W. West, Phys. Rev. Lett. **24**, 383 (1970).

[35] J. W. Allen, L. I. Johansson, I. Lindau, and S. B. Hagstrom, Phys. Rev. B **21**, 1335 (1980).

[36] J. M. Tarascon, Y. Ishikawa, B. Chevalier, J. Etourneau, P. Hagenmuller, and M. Kasaya, J. Phys. **41**, 1141 (1980).

[37] M. Mizumaki, S. Tsutsui, and F. Iga, J. Phys.: Conf. Ser. **176**, 012034 (2009).

[38] H. Hayashi, N. Kanai, N. Kawamura, M. Mizumaki, K. Imura, N. K. Sato, H. S. Suzuki, and F. Iga, J. Anal. At. Spectrom. **28**, 373 (2013).

[39] P. Lutz, M. Thees, T. R. F. Peixoto, B. Y. Kang, B. K. Cho, C.-H. Min, and F. Reinert, Philos. Mag. **96**, 3307 (2016).

[40] A. Yamasaki, A. Sekiyama, S. Imada, M. Tsunekawa, C. Dallera, L. Braicovich, T. L. Lee, A. Ochiai, and S. Suga, J. Phys. Soc. Jpn. **74**, 2538 (2005).

[41] A. Yamasaki, S. Imada, H. Higashimichi, H. Fujiwara, T. Saita, T. Miyamachi, A. Sekiyama, H. Sugawara, D. Kikuchi, H. Sato, A. Higashiya, M. Yabashi, K. Tamasaku, D. Miwa, T. Ishikawa, and S. Suga, Phys. Rev. Lett. **98**, 156402 (2007).

[42] J. Weinen, T. C. Koethe, C. F. Chang, S. Agrestini, D. Kasinathan, Y.-F. Liao, H. Fujiwara, C. S. ler-Langeheine, F. Strigari, T. Haupricht, G. Panaccione, F. Offi, G. Monaco, S. Huotari, K.-D. Tsuei, and L. H. Tjeng, J. Electron Spectrosc. Relat. Phenom. **198**, 6 (2015).

[43] M. W. Haverkort, M. Zwierzycki, and O. K. Andersen, Phys. Rev. B **85**, 165113 (2012).

[44] A. Tanaka and T. Jo, J. Phys. Soc. Jpn. **63**, 2788 (1994).

[45] G. Sawatzky and R. Green, in *Quantum Materials: Experiments and Theory*, edited by E. Pavarini, E. Koch, J. van den Brink, and G. Sawatzky (Forschungszentrum Jülich, Jülich, 2016), pp. 1.1–1.35.

[46] The values of the F and G Slater integrals and the spin-orbit interaction (ζ) used for the atomic multiplet calculations were obtained by Cowan's atomic Hartree-Fock (HF) program [58]. The obtained HF values are reduced to 84% and 88% for the simulations of the Sm^{2+} and Sm^{3+} $3d$ spectra, respectively. The parameters of the $3d^{10}4f^6$ and $3d^94f^6$ configurations in the simulations of the Sm^{2+} $3d$ spectra are $(F_f^2,F_f^4,F_f^6,\zeta_f) = (10.52,6.56,4.71,0.131)$ and $(F_f^2,F_f^4,F_f^6,\zeta_f) = (12.09,7.60,5.47,0.167)$, respectively, and $(F_{fd}^2,F_{fd}^4,G_{fd}^1,G_{fd}^3,G_{fd}^5,\zeta_d) = (7.57,3.50,5.34,3.13,2.16,10.35)$. The parameters of the $3d^{10}4f^5$ and $3d^94f^5$ configurations in the simulation of the Sm^{3+} $3d$ spectra are $(F_f^2,F_f^4,F_f^6,\zeta_f) = (12.01,7.54,5.42,0.144)$ and $(F_f^2,F_f^4,F_f^6,\zeta_f) = (13.48,8.52,6.14,0.181)$, respectively, and $(F_{fd}^2,F_{fd}^4,G_{fd}^1,G_{fd}^3,G_{fd}^5,\zeta_d) = (8.48,3.96,6.05,3.55,2.45,10.35)$. All values are in units of eV. The simulated spectra are convoluted with a Lorentzian function with FWHM = 0.19 and 0.21 eV for Sm^{2+} $3d_{5/2}$ and $3d_{3/2}$, and 0.45 eV for Sm^{3+} $3d$, respectively, and a Gaussian function with FWHM = 0.22 eV. In addition, a Mahan function with $\alpha = 0.15$ [59] is used to account for the asymmetry of the line shapes.

[47] P. A. Alekseev, V. N. Lazukov, R. Osborn, B. D. Rainford, I. P. Sadikov, E. S. Konovalova, and Yu. B. Paderno, Europhys. Lett. **23**, 347 (1993).

[48] P. A. Alekseev, J. M. Mignot, J. Rossat-Mignod, V. N. Lazukov, I. P. Sadikov, E. S. Konovalova, and Yu. B. Paderno, J. Phys.: Condens. Matter **7**, 289 (1995).

[49] D. Mandrus, J. L. Sarrao, A. Lacerda, A. Migliori, J. D. Thompson, and Z. Fisk, Phys. Rev. B **49**, 16809 (1994).

[50] O. Sakai, Y. Shimizu, and T. Kasuya, Prog. Theor. Phys. Suppl. **108**, 73 (1992).

[51] S. Tanuma, C. J. Powell, and D. R. Penn, Surf. Interface Anal. **21**, 165 (1994).

[52] M. B. Trzhaskovskaya, V. I. Nefedov, and V. G. Yarzhemsky, At. Data Nucl. Data Tables **77**, 97 (2001).

[53] M. B. Trzhaskovskaya, V. I. Nefedov, and V. G. Yarzhemsky, At. Data Nucl. Data Tables **82**, 257 (2002).

[54] M. B. Trzhaskovskaya, V. K. Nikuli, V. I. Nefedov, and V. G. Yarzhemsky, At. Data Nucl. Data Tables **92**, 245 (2006).

[55] K. Koepernik and H. Eschrig, Phys. Rev. B **59**, 1743 (1999).

[56] D. Kasinathan, K. Koepernik, L. H. Tjeng, and M. W. Haverkort, Phys. Rev. B **91**, 195127 (2015).

[57] V. N. Antonov, B. N. Harmon, and A. N. Yaresko, Phys. Rev. B **66**, 165209 (2002).

[58] R. D. Cowan, *The Theory of Atomic Structure and Spectra* (University of California Press, Berkeley, 1981).

[59] G. D. Mahan, Phys. Rev. B **11**, 4814 (1975).

[60] For the estimation of the thickness of the surface region, we used $v_{\mathrm{bulk}} = 2.549$ and 2.635 at 20 K and 250 K and $v_{\mathrm{av}} = 2.605$ and 2.681 at 20 K and 250 K, respectively. These are the same values as listed in the text, but are now presented with one digit more as they come out from the fitting analysis. Although the error bar for the absolute value of the estimated Sm valence is 0.02, the ratio of the valences may benefit from a more accurate representation since systematic errors in the fitting analysis may cancel out.

[61] M. Loewenhaupt and M. Prager, Z. Phys. B **62**, 195 (1986).

[62] D. A. Shirley, Phys. Rev. B **5**, 4709 (1972).